

Inhibition of Cell Motility by Cell-Penetrating Dynamic Covalent Cascade Exchangers: Integrins Participate in Thiol-Mediated Uptake

Filipe Coelho, Saidbakhrom Saidjalolov, Dimitri Moreau, Oliver Thorn-Seshold, and Stefan Matile*



Cite This: *JACS Au* 2023, 3, 1010–1016



Read Online

ACCESS |

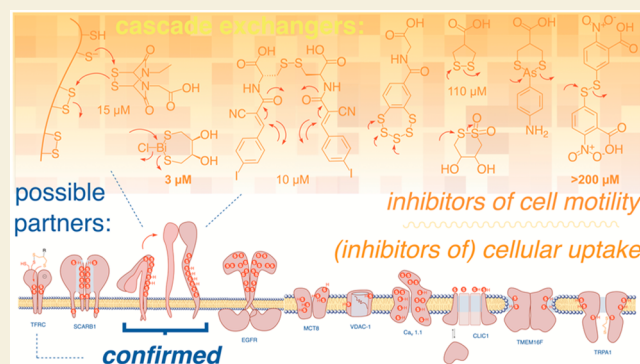
Metrics & More

Article Recommendations

Supporting Information

ABSTRACT: Integrins are cell surface proteins responsible for cell motility. Inspired by the rich disulfide exchange chemistry of integrins, we show here the inhibition of cell migration by cascade exchangers (CAXs), which also enable and inhibit cell penetration by thiol-mediated uptake. Fast-moving CAXs such as reversible Michael acceptor dimers, dithiabismepanes, and bioinspired epidthiodiketopiperazines are best, much better than Ellman's reagent. The implication that integrins participate in thiol-mediated uptake is confirmed by reduced uptake in integrin-knockdown cells. Although thiol-mediated uptake is increasingly emerging as a unifying pathway to bring matter into cells, its molecular basis is essentially unknown. These results identify the integrin superfamily as experimentally validated general cellular partners in the dynamic covalent exchange cascades that are likely to account for thiol-mediated uptake. The patterns identified testify to the complexity of the dynamic covalent networks involved. This work also provides chemistry tools to explore cell motility and expands the drug discovery potential of CAXs from antiviral toward antithrombotic and antitumor perspectives.

KEYWORDS: cell motility, thiol-mediated uptake, integrins, inhibitors, dynamic covalent inhibitors



Integrins are cell surface proteins in charge of cell adhesion, cell motility, and bidirectional signaling.^{1,2} Because of their involvement in wound healing, thrombosis,³ and cancer cell migration⁴ as well as viral entry^{5–10} and drug delivery,¹¹ they are of great interest as drug targets.² In vertebrates, the integrin superfamily consists of 24 heterodimers, all composed of α and β subunits (Figure 1A). They interact with different components of the extracellular matrix. During cell adhesion and migration, integrins change from a bent to a linear conformation. This change is controlled by one of the most beautiful disulfide tracks in biology, composed of 20 disulfides in the β subunit (Figure 1B).^{12–15} Several of these disulfides are allosteric in nature and in a hook or staple conformation,^{3,16} and literature describing dithiol/disulfide redox regulation of integrin function is increasingly emerging.^{4,17–20}

Admiring their disulfide tracks, we thought that integrins would be perfect exchange partners in thiol-mediated uptake (TMU). TMU^{21–25} refers to the cell-penetrating activity provided by thiol/disulfide cascade exchanger (CAX) motifs. CAXs undergo dynamic covalent exchanges with membrane-bound protein thiols (or disulfides), where each exchange produces a new (or offers another) covalently tethered exchanger, that can continue exchanging until they are delivered into the cytosol.²¹ TMU has been realized with many classes of CAX for the cytosolic delivery of small molecules,^{21,26} antibodies²² and other proteins,^{27–30} genome

editing machinery³¹ and other oligonucleotides,^{32–37} polymers,³⁸ liposomes,³⁹ and nanoparticles^{22,40,41} into various cellular targets including deep tissue,^{30,33} living animals,^{31,42} plant cells,³⁵ and bacteria.²⁶ Proteomics data,⁴³ heatmap patterns,^{44,45} and literature on oligonucleotide phosphorothioate^{37,46} and viral uptake^{8,47–50} all support that multipartner exchange networks are involved in how TMU brings matter into cells.²¹ However, the dynamic covalent exchange cascades of TMU are complex and its fleeting intermediates are elusive, which is likely the reason why TMU is not better known and understood.²¹

Importantly, CAX-induced TMU can be inhibited by treating cells with surface-thiol-reactive agents.^{51,52} Given that thiol-rich integrins are natively poised for reversible thiol modifications,^{3,4,16–20} we hypothesized that CAXs which enable or inhibit TMU could also inhibit the cell motility for which integrin dynamics are crucial, which in turn would

Received: March 8, 2023

Revised: April 5, 2023

Accepted: April 5, 2023

Published: April 12, 2023



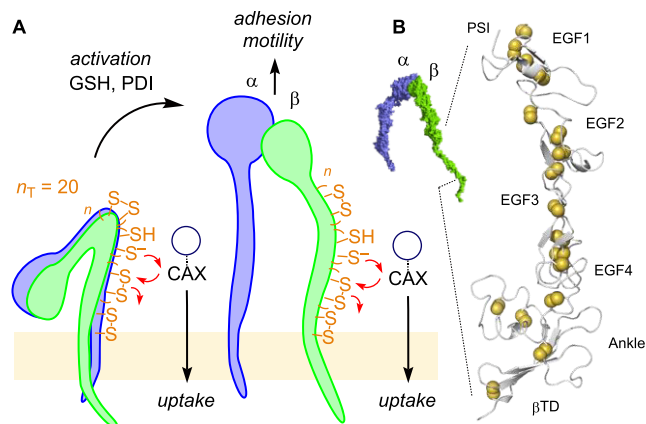


Figure 1. (A) Schematic structure of integrins in inactive (left) and active form (right), highlighting thiol-mediated activation of motility and our hypothesis of TMU by CAX moving along integrin disulfide tracks. (B) Integrins modeled from Protein Data Bank data (PDB entries 3fcs, 2vdo, 2k9j, 2h7d), zoomed onto the disulfide track and indicating domains (yellow, disulfides; TD, tail domain; EGF, epithelial growth factor; PSI, plexin–semaphorin–integrin).^{12–15}

demonstrate the involvement of integrins as one of the so far essentially unknown cellular exchange partners in TMU.

To test the effects of TMU inhibitors on cellular integrin functions, compounds 1–16 were bought or synthesized following reported procedures (Figures 2 and S2).^{44,45,51–55} Cell motility assays⁴ were adapted to automated high-content high-throughput (AHCHT) imaging methods.^{45,51} Before cell seeding, 96-well plates were coated with one of three proteins that interact with different integrins: Collagen I (C), which activates mainly β_1 -containing integrins; fibronectin (F), which activates mainly β_1 - and β_3 -containing integrins; and vitronectin (V), which activates mainly β_3 - and β_5 -containing integrins.^{1–4} HeLa Kyoto (HK), MCF-7, and MDA-MB-231 cells were then seeded on the protein-coated wells to test their migration behavior when treated with TMU inhibitors. Among many possibilities, highly aggressive MDA-MB-231 and noninvasive MCF-7 breast cancer cells were selected as established standards to explore motility⁴ and HK cells as a link to uptake⁴⁵ and to probe the power of AHCHT assays to detect small changes accurately.

The confluent cell monolayers were scraped to create “scratches” with widths of around 1 mm using a homemade device that removes cells without damaging the coating (Figure S1), as demonstrated by the different intrinsic motilities of different cells on different coatings (e.g., Figure S14). Cells were then incubated with TMU inhibitor candidates from $t = 0$, and the cell motility m was determined from the change of cell-free area A from that at $t = 0$ ($m = A_0 - A_t$) (Figures 3A,B and S8–S28).

A complex segmentation pipeline was developed to generate unbiased image masks to estimate A_t (Figures S4–S6). This AHCHT motility assay was particularly powerful with slower moving cells that are otherwise not easily distinguishable (Figures S22–S28). At least at the beginning, the motility kinetics showed quasi-linear behavior for all inhibitors (Figures 3B and S8–S28). The time dependence of the dose–response curves suggested that the results would be most reproducibly assessed after 2 h (Figures 3C,D). At least at low serum concentrations (0–2.5% FBS; Figures S7 and S29–38), single-cell mobility experiments confirmed that the observed area

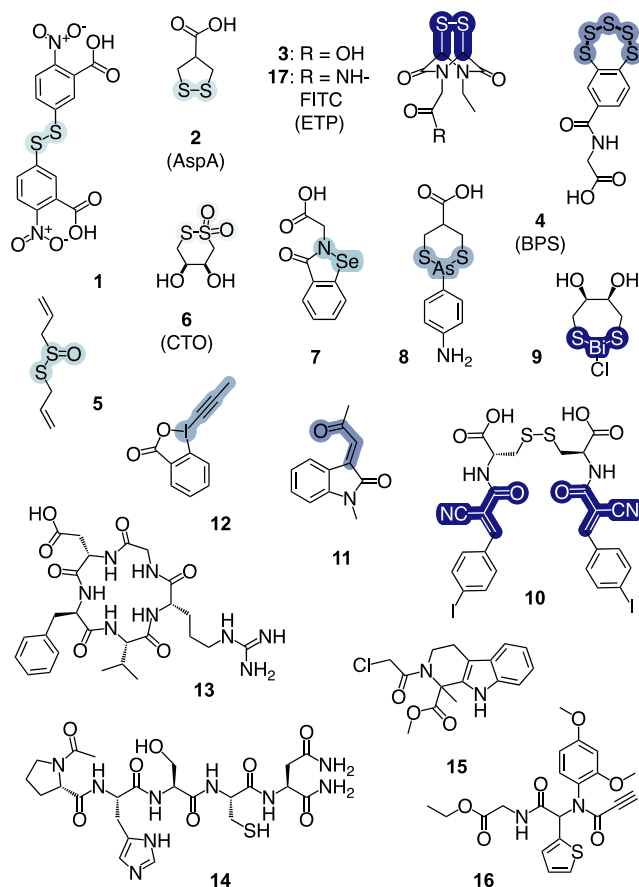


Figure 2. Dynamic covalent inhibitor candidates 1–11 and irreversible 12 ordered by relays (1–7, chalcogens; 8 and 9, pnictogens; 10–12, tetrels) and activity (increasing left to right, darkening blue; Figure 3G), above established integrin (13, 14) and PDI inhibitors (15, 16). Full structure of TMU reporter 17: Figure S2.

changes originate from motility and not from cell growth. For instance, the movement of single MDA-MB-231 cells on collagen I decelerated from $1.00 \pm 0.05 \mu\text{m min}^{-1}$ (Figure 3E) to $0.40 \pm 0.01 \mu\text{m min}^{-1}$ with $3 \mu\text{M}$ inhibitor 9 (Figure 3F). This decrease matched the formal wound healing times to close a 1 mm scratch (17 h against 40 h). Because it was important to avoid misinterpretation of cell death as motility inhibition,⁵⁶ CAXs and controls 1–12 were reconfirmed^{45,51–53} as nontoxic under the experimental conditions (Figure S3).

Cell migration inhibition by 1–16 was assessed for the three cell lines on all three surfaces (Figures S8–S28 and Tables S1–S8). Heatmaps comparing values of IC_{50} or MIC (calculated as IC_{15} ; see eq S2) were constructed (Figures 3G and S40). The difference between IC_{50} and MIC tracked to the switching half-window C_R ^{57,58} a metric that can report on cooperativity (large C_R indicates negative cooperativity), or on whether several active sites⁵⁸ are involved in an exchange cascade (Figure S41). Fractional heatmaps (Figure 3H,I) and two-component correlations (Figure 3J) were extracted to test for patterns (e.g., inhibitors with similar targets).

Most candidates inhibited the migration of all tested cells on most surfaces, even in the presence of serum (Figures 3G and S8–S37). The selectivity patterns varied between CAXs (heatmap rows), cell types, and surfaces (heatmap columns)

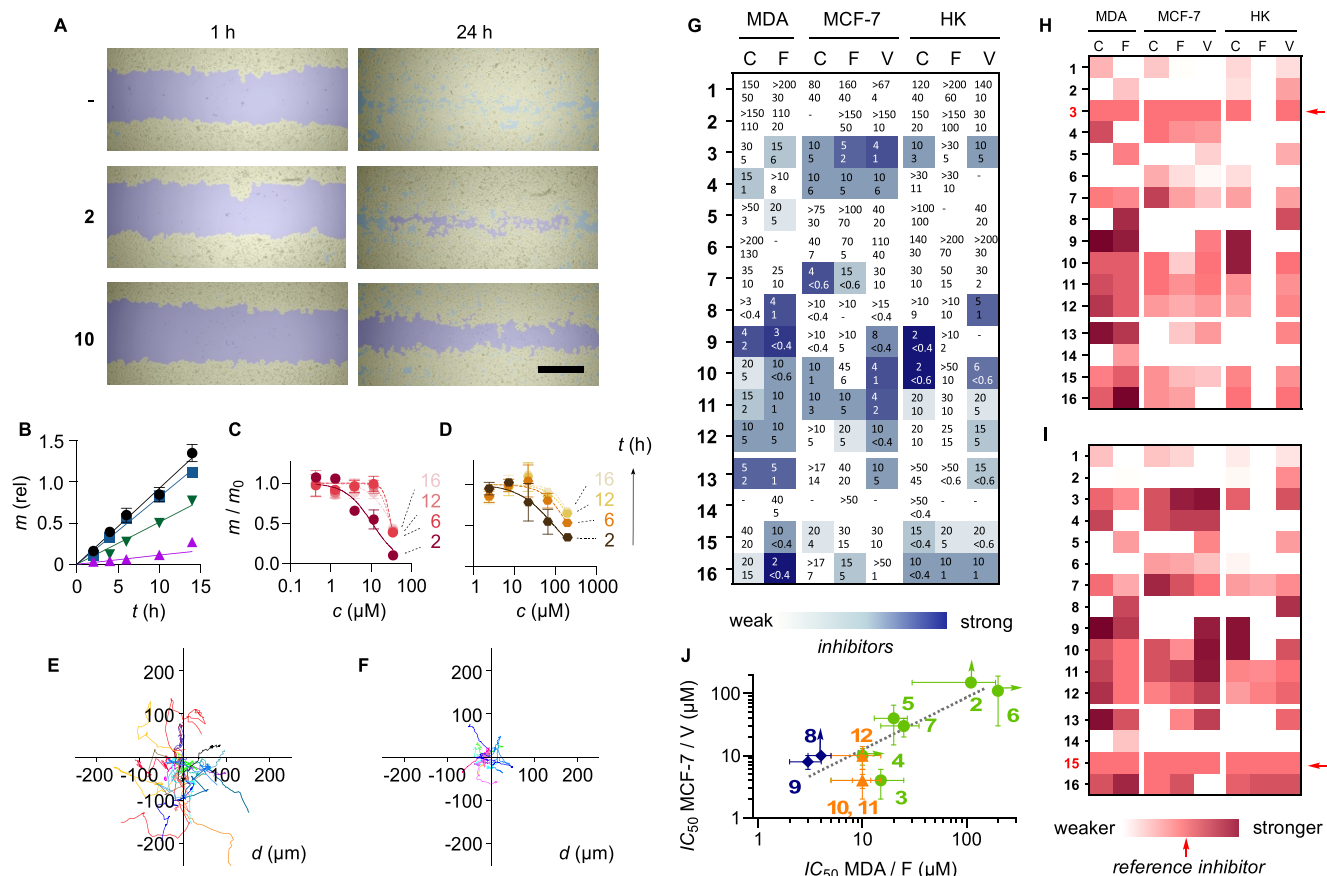


Figure 3. (A) Original transmitted light images for MDA-MB-231 cells on collagen I-coated surfaces without (top) and with inhibitors **2** ($150 \mu\text{M}$) and **10** ($5 \mu\text{M}$) 1 and 24 h after scratching, overlaid with automatically generated image masks for cells (yellow) and cell-free area originating from scratch (area = A, blue) or interstitial space (cyan). Scale bar: 1 mm. (B) Motility m of MDA-MB-231 cells on collagen with **2** (blue squares, $150 \mu\text{M}$), **7** (green downward triangles, $50 \mu\text{M}$), or **10** (purple upward triangles, $50 \mu\text{M}$) or without inhibitor (black circles, $=m_0$). (C, D) Relative motility m/m_0 on collagen for (C) HK cells with **3** and (D) MCF-7 cells with **6** as a function of concentration and time. (E, F) Wind-rose plots with tracks of single MDA-MB-231 cells on collagen I in the (E) absence and (F) presence of **9** ($3 \mu\text{M}$). (G) Heatmap for the inhibition of the motility of MDA-MB-231, MCF-7, and HK cells on collagen I [C], fibronectin [F], and vitronectin [V] by inhibitor candidates **2–12** and controls (**1**, **13–16**), measured 2 h after addition at varied concentrations to determine IC_{50} (top) and MIC ($=\text{IC}_{15}$, bottom), both in μM . “–”: inactive. (H) Fractional heatmap against **3**. (I) Fractional heatmap against **15**, arrows indicate the reference inhibitors. (J) Two-component correlation of MDA-MB-231 cells on fibronectin against MCF-7 on vitronectin (green circles, chalcogens; blue diamonds, pnictogens; orange triangles, tetrels; error bars, SEM; upward and rightward arrows indicate the actual values to be much higher).

(Figure 3G–I). Most CAXs were much more active than the known Ellman reagent **1**.⁴ The inhibition enhancement ($\text{IE} = \text{IC}_{50}(\text{1})/\text{IC}_{50}(\text{test})$) reached ≥ 70 for chlorodithiobismepane **9**⁵³ halting the aggressive MDA-MB-231 cells on fibronectin or **32** for the bioinspired epidithiodiketopiperazine (ETP)^{51,55} **3** inhibiting MCF-7 cells on the same surface. The typically most efficient CAXs for TMU, such as **9**, **10**, and **3**, gave inhibition that could be up to 10 times more potent than established non-covalent integrin inhibitors such as cyclic RGD **13**,^{6,59,60} $\alpha_3\beta_1$ -selective anti-SARS-CoV-2 **14**,^{2,61,62} and protein disulfide isomerase (PDI) inhibitors **15** and **16** (Figure 3G,H).^{63–65}

Fractional heatmaps weighted against ETP **3** highlighted, for instance, its selectivity for MCF-7 cells on all surfaces and the high activity of pnictogen- and tetrel-centered CAXs **8–12** against the aggressive MDA-MB-231 cells (Figure 3H). For every cell type on every surface, at least one CAX outperformed the benchmark covalent PDI inhibitor **15**, and the nature of those CAXs varied (exception: HK on F; Figure 3I). Focused two-component correlations are an alternative tool to recognize selectivity, as exemplified here with MDA on F against MCF-7 on V (Figure 3J).

The appearance of unique patterns with distinct hotspots supported that CAX inhibitors operate selectively, beyond global reactivity, with specific mechanisms and therefore have a certain drug discovery potential. The most antimigratory CAXs such as **3**, **9**, and **10** contain highly reactive, fast-exchanging chalcogen-, pnictogen-, and tetrel-centered relays. Those CAXs that are typically excellent for TMU but underperformed in the antimigratory assay were those that (i) produce slow-exchanging, “sticky” dynamic covalent networks that excel for cytosolic delivery, like the bioinspired benzopolysulfane (BPS)⁵⁴ **4**, (ii) exchange only in aprotic hydrophobic environments like cyclic thiosulfonate (CTO)⁴⁴ **6**, or (iii) may prefer to exchange with other protein partners, such as asparagusic acid (AspA) **2** with the transferrin receptor.⁴³ These trends were consistent with the hypothesis that the inhibition of cell motility by the most efficient CAXs operates with fast exchange cascades along thiol or disulfide arrays on cell surfaces.

Good inhibitors of cell motility were overall good inhibitors of thiol-mediated uptake (Figure 4A,B). Comparison with literature IC_{50} for the inhibition of TMU of **17** (ETP **3** with an

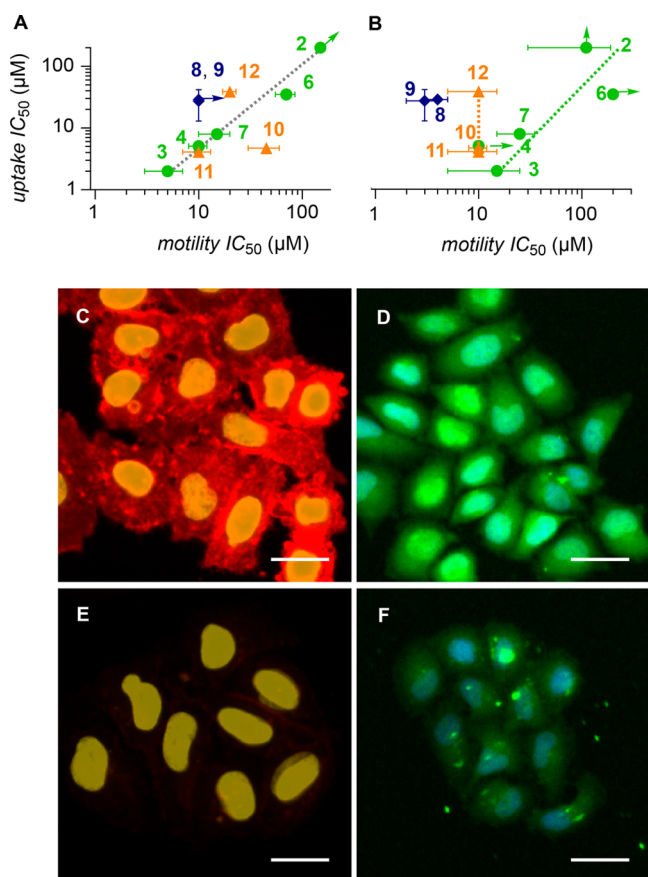


Figure 4. (A) IC_{50} of 2–12 for MCF-7 cell motility on fibronectin compared to their IC_{50} for TMU of 17 into HK cells. (B) Similar IC_{50} comparison for MDA-MB-231 cell motility on fibronectin (symbols as in Figure 3J). Uptake data from refs 44, 45, 51–53. (C–F) Fluorescence microscopy images of (C, D) wild-type and (E, F) INT β_1 siRNA knockdown HK cells incubated with (C, E) immunofluorescence integrin probe (red) and (D, F) 17 (green) (yellow, blue: Hoechst 33342, nuclei; scale bars, 30 μm).

attached fluorophore)⁵⁵ into HK cells with the motility of MCF-7 and MDA-MB-231 cells on fibronectin gave distinct patterns with weakly linear correlations (dashed lines) that included either all or only chalcogen-centered CAXs. However, these and other low-confidence patterns are not further discussed here, to avoid overinterpretations.

To close the functional feedback loop, β_1 integrins were knocked down in HK cells, as confirmed by immunofluorescence quantification (Figure 4C vs E). Cellular uptake of fluorescent ETP 17 into the cytosol and mostly the nucleus,⁵⁵ determined under routine conditions,⁵⁵ decreased significantly in the absence of β_1 integrins (Figure 4D,F). As far as we know, this difference provides the first direct experimental support that integrins act as dynamic covalent exchange partners in thiol-mediated uptake. The complementary motility inhibition could not be measured because the motility of knockdown cells was as poor as expected, reappearing only when integrins were starting to be re-expressed (not shown).

In summary, we report that a focused collection of CAXs inhibits the motility of various cells on various surfaces. Their antimigratory activities exceed that of Ellman's reagent by far and correlates globally with their abilities to penetrate cells and deliver substrates into the cytosol. Knockdown experiments

support the conclusion that the same proteins are involved in TMU as in the antimigratory effect.

This conclusion is important. Despite the rich collection of candidates,²¹ only one TMU partner had previously been robustly identified, i.e., the transferrin receptor, without being general (for AspA,⁴³ not ETP⁵⁵). Now we find that the integrin superfamily is the first general exchange partner that has experimental support to participate in TMU. These results thus (a) introduce dynamic covalent cascade exchange chemistry to the control of cell motility, (b) expand the CAX drug discovery space from antiviral toward antithrombotic and antitumor potential, (c) confirm integrins as exchange partners in the dynamic TMU networks that deliver matter into cells, from drugs to pathogens, and thus (d) inspire new design strategies (e.g., multivalent CAXs³⁰ to benefit from integrin clustering⁶⁶). These lessons are likely to enable significant and varied future advances.

METHODS

Automated Cell Motility Inhibition Assay

On a 96-well Black ibiTreat sterile microplate coated with collagen I, fibronectin, or vitronectin (see the Supporting Information), HeLa Kyoto, MCF-7 (6×10^4 cells/well), or MDA-MB-231 cells (9×10^4 cells/well) were seeded in DMEM + 10% FBS and kept overnight at 37 °C under 5% CO₂ atmosphere. The cell monolayers were scraped with a homemade device (Figure S1) and washed twice with PBS. Then the medium was changed to DMEM (with FBS 0–7.5%), and the inhibitor candidates were added with an electronic multichannel pipet. With an automated confocal microscope, transmitted light (TL) images were recorded at the center of the wells, and time series of 14–26 h were recorded. The onset of toxicity at high inhibitor concentrations was identified by dead rounded-up cells that detached and accumulated in the center of the scratch (Figure S3A), and measurements were limited to concentrations below this threshold (Figure S3B).

Automated analysis processed the original time-lapse TL images (Figure S4A) to generate a relevant mask of the cell layer. The first set of masks determined the cell edge (Figure S4C). This was done by top-hat modification of the TL image that highlights the cell boundaries (Figure S4B). To the segmented image, a size filter was applied to exclude any object below 50 μm^2 (Figure S4D). Following a similar procedure on a pixel-intensity-inverted image (Figure S5A,B), the cell body was segmented (Figure S5C). Finally, the two cell masks, that is, the cell edge (Figure S4D) and cell body (Figure S5C), were combined to create the cell layer (Figure S6A). This cell layer was then slightly grown to give a homogeneous layer (Figure S6B). Since the growth led to the appearance of some unwanted background objects, a size filter was added to remove all objects below 30 000 μm^2 to give the final cell layer (Figure S6C). To determine the scratch area, the cell layer (Figure S6C) was subtracted from the whole image mask (including all pixels of the image, Figure S6D) to give the desired area (Figure S6E).

In the final image (Figure S6F), the area of the scratch (A) was deduced from the blue area, the cell layer was labeled in yellow, and the space between cells not caused by the scratch (interstitial space) was labeled in cyan. The motility m was calculated by subtracting the area of the blue layer at a specific time (A_t) from the area at $t = 0$ (A_0), i.e., $m = A_0 - A_t$ and

normalized against m_0 under the same conditions without inhibitor. Duplicates were performed for each condition and averaged. The relative motility m/m_0 was plotted as a function of the inhibitor concentration and fitted to the Hill equation to retrieve IC_{15} (MIC), IC_{50} , and n .

■ ASSOCIATED CONTENT

SI Supporting Information

The Supporting Information is available free of charge at <https://pubs.acs.org/doi/10.1021/jacsau.3c00113>.

Materials and methods; inhibitor synthesis; cell culture; coating procedures; expanded cell motility imaging procedure; expanded AHCHT motility analysis; dependence on inhibitors, concentration, time, cells, surfaces, and serum; pattern generation; single-cell motility inhibition procedure; ITGB1 knockdown; cellular uptake inhibition procedure (PDF)

Video of AHCHT motility assay with inhibitor 9 (MPG)

Video of AHCHT motility assay without inhibitor (MPG)

■ AUTHOR INFORMATION

Corresponding Author

Stefan Matile – Department of Biochemistry, University of Geneva, 1211 Geneva, Switzerland; orcid.org/0000-0002-8537-8349; Email: stefan.matile@unige.ch

Authors

Filipe Coelho – Department of Organic Chemistry, University of Geneva, 1211 Geneva, Switzerland

Saidbakhrom Saidjalolov – Department of Organic Chemistry, University of Geneva, 1211 Geneva, Switzerland

Dimitri Moreau – Department of Biochemistry, University of Geneva, 1211 Geneva, Switzerland

Oliver Thorn-Seshold – Department of Pharmacy, Ludwig-Maximilians University of Munich, 81377 Munich, Germany; orcid.org/0000-0003-3981-651X

Complete contact information is available at <https://pubs.acs.org/10.1021/jacsau.3c00113>

Notes

The authors declare no competing financial interest.

■ ACKNOWLEDGMENTS

We thank B. Lim, X.-X. Cheng, T. Kato, and the group of J. Waser for contributions to inhibitor synthesis; B. Pologne and S. Vossio for assistance; the NMR, MS, ACCESS and Bioimaging platforms for services; and the University of Geneva, the National Centre of Competence in Research (NCCR) Chemical Biology (51NF40-185898), the NCCR Molecular Systems Engineering (51NF40-182895), and the Swiss NSF (Swiss-ERC Advanced Grant TIMEUP, TMAG-2_209190; Excellence Grant 200020 204175) for financial support.

■ REFERENCES

(1) Hynes, R. O. Integrins: Bidirectional, Allosteric Signaling Machines. *Cell* **2002**, *110*, 673–687.

(2) Slack, R. J.; Macdonald, S. J. F.; Roper, J. A.; Jenkins, R. G.; Hatley, R. J. D. Emerging Therapeutic Opportunities for Integrin Inhibitors. *Nat. Rev. Drug Discovery* **2022**, *21*, 60–78.

(3) Mor-Cohen, R. Disulfide Bonds as Regulators of Integrin Function in Thrombosis and Hemostasis. *Antioxid. Redox Signaling* **2016**, *24*, 16–31.

(4) Popielarski, M.; Ponamarczuk, H.; Stasiak, M.; Watała, C.; Świątkowska, M. Modifications of Disulfide Bonds in Breast Cancer Cell Migration and Invasiveness. *Am. J. Cancer Res.* **2019**, *9*, 1554–1582.

(5) Hussein, H. A. M.; Walker, L. R.; Abdel-Raouf, U. M.; Desouky, S. A.; Montasser, A. K. M.; Akula, S. M. Beyond RGD: Virus Interactions with Integrins. *Arch. Virol.* **2015**, *160*, 2669–2681.

(6) Tomassi, S.; D'Amore, V. M.; Di Leva, F. S.; Vannini, A.; Quilici, G.; Weinmüller, M.; Reichart, F.; Amato, J.; Romano, B.; Izzo, A. A.; Di Maro, S.; Novellino, E.; Musco, G.; Gianni, T.; Kessler, H.; Marinelli, L. Halting the Spread of Herpes Simplex Virus-1: The Discovery of an Effective Dual $\alpha_v\beta_6/\alpha_v\beta_8$ Integrin Ligand. *J. Med. Chem.* **2021**, *64*, 6972–6984.

(7) Bugatti, K. $\alpha_v\beta_6$ Integrin: An Intriguing Target for COVID-19 and Related Diseases. *ChemBioChem* **2021**, *22*, 2516–2520.

(8) Suzuki, S.; Geri, J. B.; Knutson, S. D.; Bell-Temin, H.; Tamura, T.; Fernández, D. F.; Lovett, G. H.; Till, N. A.; Heller, B. L.; Guo, J.; MacMillan, D. W. C.; Ploss, A. Photochemical Identification of Auxiliary Severe Acute Respiratory Syndrome Coronavirus 2 Host Entry Factors Using μ Map. *J. Am. Chem. Soc.* **2022**, *144*, 16604–16611.

(9) Dakal, T. C. SARS-CoV-2 Attachment to Host Cells Is Possibly Mediated via RGD-Integrin Interaction in a Calcium-Dependent Manner and Suggests Pulmonary EDTA Chelation Therapy as a Novel Treatment for COVID 19. *Immunobiology* **2021**, *226*, 152021.

(10) Sigrist, C. J.; Bridge, A.; Le Mercier, P. A Potential Role for Integrins in Host Cell Entry by SARS-CoV-2. *Antiviral Res.* **2020**, *177*, 104759.

(11) Arosio, D.; Casagrande, C. Advancement in Integrin Facilitated Drug Delivery. *Adv. Drug Delivery Rev.* **2016**, *97*, 111–143.

(12) Springer, T. A.; Zhu, J.; Xiao, T. Structural Basis for Distinctive Recognition of Fibrinogen γ C Peptide by the Platelet Integrin $\alpha_{IIb}\beta_3$. *J. Cell Biol.* **2008**, *182*, 791–800.

(13) Zhu, J.; Luo, B.-H.; Xiao, T.; Zhang, C.; Nishida, N.; Springer, T. A. Structure of a Complete Integrin Ectodomain in a Physiologic Resting State and Activation and Deactivation by Applied Forces. *Mol. Cell* **2008**, *32*, 849–861.

(14) Lau, T.-L.; Kim, C.; Ginsberg, M. H.; Ulmer, T. S. The Structure of the Integrin $\alpha_{IIb}\beta_3$ Transmembrane Complex Explains Integrin Transmembrane Signalling. *EMBO J.* **2009**, *28*, 1351–1361.

(15) Wegener, K. L.; Partridge, A. W.; Han, J.; Pickford, A. R.; Liddington, R. C.; Ginsberg, M. H.; Campbell, I. D. Structural Basis of Integrin Activation by Talin. *Cell* **2007**, *128*, 171–182.

(16) Chiu, J.; Hogg, P. J. Allosteric Disulfides: Sophisticated Molecular Structures Enabling Flexible Protein Regulation. *J. Biol. Chem.* **2019**, *294*, 2949–2908.

(17) Passam, F.; Chiu, J.; Ju, L.; Pijning, A.; Jahan, Z.; Mor-Cohen, R.; Yeheskel, A.; Kolšek, K.; Thärichen, L.; Aponte-Santamaria, C.; Gräter, F.; Hogg, P. J. Mechano-Redox Control of Integrin De-adhesion. *eLife* **2018**, *7*, e34843.

(18) Lorenzen, I.; Eble, J. A.; Hanschmann, E.-M. Thiol Switches in Membrane Proteins - Extracellular Redox Regulation in Cell Biology. *Biol. Chem.* **2021**, *402*, 253–269.

(19) Lahav, J.; Jurk, K.; Hess, O.; Barnes, M. J.; Farndale, R. W.; Luboshitz, J.; Kehrel, B. E. Sustained Integrin Ligation Involves Extracellular Free Sulfhydryls and Enzymatically Catalyzed Disulfide Exchange. *Blood* **2002**, *100*, 2472–2478.

(20) Laragione, T.; Bonetto, V.; Casoni, F.; Massignan, T.; Bianchi, G.; Gianazza, E.; Ghezzi, P. Redox Regulation of Surface Protein Thiols: Identification of Integrin α_4 as a Molecular Target by Using Redox Proteomics. *Proc. Natl. Acad. Sci. U. S. A.* **2003**, *100*, 14737–14741.

- (21) Laurent, Q.; Martinent, R.; Lim, B.; Pham, A.-T.; Kato, T.; López-Andarias, J.; Sakai, N.; Matile, S. Thiol-Mediated Uptake. *JACS Au* **2021**, *1*, 710–728.
- (22) Du, S.; Liew, S. S.; Li, L.; Yao, S. Q. Bypassing Endocytosis: Direct Cytosolic Delivery of Proteins. *J. Am. Chem. Soc.* **2018**, *140*, 15986–15996.
- (23) Zhou, J.; Shao, Z.; Liu, J.; Duan, Q.; Wang, X.; Li, J.; Yang, H. From Endocytosis to Nonendocytosis: The Emerging Era of Gene Delivery. *ACS Appl. Bio Mater.* **2020**, *3*, 2686–1701.
- (24) Ulrich, S. Growing Prospects of Dynamic Covalent Chemistry in Delivery Applications. *Acc. Chem. Res.* **2019**, *52*, 510–519.
- (25) Torres, A. G.; Gait, M. J. Exploiting Cell Surface Thiols to Enhance Cellular Uptake. *Trends Biotechnol.* **2012**, *30*, 185–190.
- (26) Shchelik, I. S.; Gademann, K. Synthesis and Antimicrobial Evaluation of New Cephalosporin Derivatives Containing Cyclic Disulfide Moieties. *ACS Infect. Dis.* **2022**, *8*, 2327–2338.
- (27) Aubry, S.; Burlina, F.; Dupont, E.; Delaroche, D.; Joliot, A.; Lavielle, S.; Chassaing, G.; Sagan, S. Cell-Surface Thiols Affect Cell Entry of Disulfide-Conjugated Peptides. *FASEB J.* **2009**, *23*, 2956–2967.
- (28) Meng, X.; Li, T.; Zhao, Y.; Wu, C. CXC-Mediated Cellular Uptake of Mini-proteins: Forsaking “Arginine Magic”. *ACS Chem. Biol.* **2018**, *13*, 3078–3086.
- (29) Lu, J.; Wang, H.; Tian, Z.; Hou, Y.; Lu, H. Cryopolymerization of 1,2-Dithiolanes for the Facile and Reversible Grafting-from Synthesis of Protein–Polydisulfide Conjugates. *J. Am. Chem. Soc.* **2020**, *142*, 1217–1221.
- (30) Martinent, R.; Tawfik, S.; López-Andarias, J.; Moreau, D.; Laurent, Q.; Matile, S. Dithiolane Quartets: Thiol-Mediated Uptake Enables Cytosolic Delivery in Deep Tissue. *Chem. Sci.* **2021**, *12*, 13922–13929.
- (31) Guo, J.; Wan, T.; Li, B.; Pan, Q.; Xin, H.; Qiu, Y.; Ping, Y. Rational Design of Poly(disulfide)s as a Universal Platform for Delivery of CRISPR-Cas9 Machinery toward Therapeutic Genome Editing. *ACS Cent. Sci.* **2021**, *7*, 990–1000.
- (32) Zhou, J.; Sun, L.; Wang, L.; Liu, Y.; Li, J.; Li, J.; Li, J.; Yang, H. Self-Assembled and Size-Controllable Oligonucleotide Nanospheres for Effective Antisense Gene Delivery through an Endocytosis-Independent Pathway. *Angew. Chem. Int. Ed.* **2019**, *58*, 5236–5240.
- (33) Kohata, A.; Hashim, P. K.; Okuro, K.; Aida, T. Transferrin-Appended Nanocapsule for Transcellular siRNA Delivery into Deep Tissues. *J. Am. Chem. Soc.* **2019**, *141*, 2862–2866.
- (34) Lang, W.; Tan, W.; Zhou, B.; Zhuang, Y.; Zhang, B.; Jiang, L.; Yao, S. Q.; Ge, J. Mitochondria-Targeted Gene Silencing Facilitated by Mito-CPDs. *Chem. Eur. J.* **2023**, *29*, No. e202204021.
- (35) Mou, Q.; Xue, X.; Ma, Y.; Banik, M.; Garcia, V.; Guo, W.; Wang, J.; Song, T.; Chen, L.-Q.; Lu, Y. Efficient Delivery of a DNA Aptamer-Based Biosensor into Plant Cells for Glucose Sensing through Thiol-Mediated Uptake. *Sci. Adv.* **2022**, *8*, eabo0902.
- (36) Shu, Z.; Tanaka, I.; Ota, A.; Fushihara, D.; Abe, N.; Kawaguchi, S.; Nakamoto, K.; Tomoi, F.; Tada, S.; Ito, Y.; Kimura, Y.; Abe, H. Disulfide-Unit Conjugation Enables Ultrafast Cytosolic Internalization of Antisense DNA and siRNA. *Angew. Chem. Int. Ed.* **2019**, *58*, 6611–6615.
- (37) Laurent, Q.; Martinent, R.; Moreau, D.; Winssinger, N.; Sakai, N.; Matile, S. Oligonucleotide Phosphorothioates Enter Cells by Thiol-Mediated Uptake. *Angew. Chem. Int. Ed.* **2021**, *60*, 19102–19106.
- (38) Bej, R.; Ghosh, A.; Sarkar, J.; Das, B. B.; Ghosh, S. Thiol-Disulfide Exchange Reaction Promoted Highly Efficient Cellular Uptake of Pyridyl Disulfide Appended Nonionic Polymers. *ChemBioChem* **2020**, *21*, 2921–2926.
- (39) Qualls, M. L.; Lou, J.; McBee, D. P.; Baccile, J. A.; Best, M. D. Cyclic Disulfide Liposomes for Membrane Functionalization and Cellular Delivery. *Chem. Eur. J.* **2022**, *28*, No. e202201164.
- (40) Kanjilal, P.; Dutta, K.; Thayumanavan, S. Thiol-Disulfide Exchange as a Route for Endosomal Escape of Polymeric Nanoparticles. *Angew. Chem. Int. Ed.* **2022**, *61*, No. e202209227.
- (41) Knoll, P.; Francesco Racaniello, G.; Laquintana, V.; Veider, F.; Saleh, A.; Seybold, A.; Denora, N.; Bernkop-Schnürch, A. Lipid-Based Nanoparticles: Enhanced Cellular Uptake via Surface Thiolation. *Int. J. Pharm.* **2023**, *635*, 122753.
- (42) Zhu, Y.; Lin, M.; Hu, W.; Wang, J.; Zhang, Z.-G.; Zhang, K.; Yu, B.; Xu, F.-J. Controllable Disulfide Exchange Polymerization of Polyguanidine for Effective Biomedical Applications by Thiol-Mediated Uptake. *Angew. Chem. Int. Ed.* **2022**, *61*, No. e202200535.
- (43) Abegg, D.; Gasparini, G.; Hoch, D. G.; Shuster, A.; Bartolami, E.; Matile, S.; Adibekian, A. Strained Cyclic Disulfides Enable Cellular Uptake by Reacting with the Transferrin Receptor. *J. Am. Chem. Soc.* **2017**, *139*, 231–238.
- (44) Kato, T.; Lim, B.; Cheng, Y.; Pham, A.-T.; Maynard, J.; Moreau, D.; Poblador-Bahamonde, A. I.; Sakai, N.; Matile, S. Cyclic Thiosulfonates for Thiol-Mediated Uptake: Cascade Exchangers, Transporters, Inhibitors. *JACS Au* **2022**, *2*, 839–852.
- (45) Lim, B.; Sakai, N.; Matile, S. Tetrel-Centered Exchange Cascades to Decouple Inhibition and Induction of Thiol-Mediated Uptake: Introducing Cell-Penetrating Thiolactones, Focus on Reversible Michael Acceptor Dimers. *Helv. Chim. Acta* **2023**, *106*, No. e202300020.
- (46) Crooke, S. T.; Seth, P. P.; Vickers, T. A.; Liang, X. The Interaction of Phosphorothioate-Containing RNA Targeted Drugs with Proteins Is a Critical Determinant of the Therapeutic Effects of These Agents. *J. Am. Chem. Soc.* **2020**, *142*, 14754–14771.
- (47) Tang, X.; Yang, M.; Duan, Z.; Liao, Z.; Liu, L.; Cheng, R.; Fang, M.; Wang, G.; Liu, H.; Xu, J.; Kamau, P. M.; Zhang, Z.; Yang, L.; Zhao, X.; Peng, X.; Lai, R. Transferrin Receptor Is Another Receptor for SARS-CoV-2 Entry. *bioRxiv* **2020**, DOI: 10.1101/2020.10.23.350348.
- (48) Sokolov, A.; Isakova-Sivak, I.; Grudinina, N.; Mezhenkaya, D.; Litasova, E.; Kostevich, V.; Stepanova, E.; Rak, A.; Sychev, I.; Kirik, O.; Rudenko, L. Ferritin II Efficiently Inhibits SARS-CoV-2 Replication in Vero Cells. *Viruses* **2022**, *14*, 317.
- (49) Koppiseti, R. K.; Fulcher, Y. G.; Van Doren, S. R. Fusion Peptide of SARS-CoV-2 Spike Rearranges into a Wedge Inserted in Bilayered Micelles. *J. Am. Chem. Soc.* **2021**, *143*, 13205–13211.
- (50) Xiu, S.; Dick, A.; Ju, H.; Mirzaie, S.; Abdi, F.; Cocklin, S.; Zhan, P.; Liu, X. Inhibitors of SARS-CoV-2 Entry: Current and Future Opportunities. *J. Med. Chem.* **2020**, *63*, 12256–12274.
- (51) Cheng, Y.; Pham, A.-T.; Kato, T.; Lim, B.; Moreau, D.; López-Andarias, J.; Zong, L.; Sakai, N.; Matile, S. Inhibitors of Thiol-Mediated Uptake. *Chem. Sci.* **2021**, *12*, 626–631.
- (52) Lim, B.; Cheng, Y.; Kato, T.; Pham, A.-T.; Le Du, E.; Mishra, A. K.; Grinhagen, E.; Moreau, D.; Sakai, N.; Waser, J.; Matile, S. Inhibition of Thiol-Mediated Uptake with Irreversible Covalent Inhibitors. *Helv. Chim. Acta* **2021**, *104*, No. e2100085.
- (53) Lim, B.; Kato, T.; Besnard, C.; Poblador Bahamonde, A. I.; Sakai, N.; Matile, S. Pnictogen-Centered Cascade Exchangers for Thiol-Mediated Uptake: As(III)-, Sb(III)-, and Bi(III)-Expanded Cyclic Disulfides as Inhibitors of Cytosolic Delivery and Viral Entry. *JACS Au* **2022**, *2*, 1105–1114.
- (54) Cheng, Y.; Zong, L.; López-Andarias, J.; Bartolami, E.; Okamoto, Y.; Ward, T. R.; Sakai, N.; Matile, S. Cell-Penetrating Dynamic-Covalent Benzopolysulfane Networks. *Angew. Chem. Int. Ed.* **2019**, *58*, 9522–9526.
- (55) Zong, L.; Bartolami, E.; Abegg, D.; Adibekian, A.; Sakai, N.; Matile, S. Epithiodiketopiperazines: Strain-Promoted Thiol-Mediated Cellular Uptake at the Highest Tension. *ACS Cent. Sci.* **2017**, *3*, 449–453.
- (56) Micoine, K.; Persich, P.; Llaveria, J.; Lam, M.-H.; Maderna, A.; Loganzo, F.; Fürstner, A. Total Syntheses and Biological Reassessment of Lactimidomycin, Isomigrastatin and Congener Glutarimide Antibiotics. *Chem. Eur. J.* **2013**, *19*, 7370–7383.
- (57) Mammen, M.; Choi, S.-K.; Whitesides, G. M. Polyvalent Interactions in Biological Systems: Implications for Design and Use of Multivalent Ligands and Inhibitors. *Angew. Chem. Int. Ed.* **1998**, *37*, 2754–2794.

- (58) Hunter, C. A.; Anderson, H. L. What Is Cooperativity? *Angew. Chem. Int. Ed.* **2009**, *48*, 7488–7499.
- (59) Hatley, R. J. D.; Macdonald, S. J. F.; Slack, R. J.; Le, J.; Ludbrook, S. B.; Lukey, P. T. An α -RGD Integrin Inhibitor Toolbox: Drug Discovery Insight, Challenges and Opportunities. *Angew. Chem. Int. Ed.* **2018**, *57*, 3298–3321.
- (60) Kapp, T. G.; Rechenmacher, F.; Neubauer, S.; Maltsev, O. V.; Cavalcanti-Adam, E. A.; Zarka, R.; Reuning, U.; Notni, J.; Wester, H.-J.; Mas-Moruno, C.; Spatz, J.; Geiger, B.; Kessler, H. A Comprehensive Evaluation of the Activity and Selectivity Profile of Ligands for RGD-Binding Integrins. *Sci. Rep.* **2017**, *7*, 39805.
- (61) Beddingfield, B. J.; Iwanaga, N.; Chapagain, P. P.; Zheng, W.; Roy, C. J.; Hu, T. Y.; Kolls, J. K.; Bix, G. J. The Integrin Binding Peptide, ATN-161, as a Novel Therapy for SARS-CoV-2 Infection. *JACC Basic Transl. Sci.* **2021**, *6*, 1–8.
- (62) Khalili, P.; Arakelian, A.; Chen, G.; Plunkett, M. L.; Beck, I.; Parry, G. C.; Doñate, F.; Shaw, D. E.; Mazar, A. P.; Rabbani, S. A. A Non-RGD-Based Integrin Binding Peptide (ATN-161) Blocks Breast Cancer Growth and Metastasis in Vivo. *Mol. Cancer Ther.* **2006**, *5*, 2271–2280.
- (63) Ge, J.; Zhang, C.-J.; Li, L.; Chong, L. M.; Wu, X.; Hao, P.; Sze, S. K.; Yao, S. Q. Small Molecule Probe Suitable for *In Situ* Profiling and Inhibition of Protein Disulfide Isomerase. *ACS Chem. Biol.* **2013**, *8*, 2577–2585.
- (64) Robinson, R. M.; Reyes, L.; Duncan, R. M.; Bian, H.; Reitz, A. B.; Manevich, Y.; McClure, J. J.; Champion, M. M.; Chou, C. J.; Sharik, M. E.; Chesi, M.; Bergsagel, P. L.; Dolloff, N. G. Inhibitors of the Protein Disulfide Isomerase Family for the Treatment of Multiple Myeloma. *Leukemia* **2019**, *33*, 1011–1022.
- (65) Powell, L. E.; Foster, P. A. Protein Disulphide Isomerase Inhibition as a Potential Cancer Therapeutic Strategy. *Cancer Med.* **2021**, *10*, 2812–2825.
- (66) Boturnyn, D.; Coll, J.-L.; Garanger, E.; Favrot, M.-C.; Dumy, P. Template Assembled Cyclopeptides as Multimeric System for Integrin Targeting and Endocytosis. *J. Am. Chem. Soc.* **2004**, *126*, 5730–5739.